Soft Matter

PAPER

Check for updates

Crystallization of semiflexible polymers in melts and solutions†

Pavel I. Kos, [ID] *[ac] Viktor A. Ivanov[ab] and Alexander V. Chertovich[ac]

We studied the crystallization of semiflexible polymer chains in melts and poor-solvent solutions with different concentrations using dissipative particle dynamics (DPD) computer simulation techniques. We used the coarse-grained polymer model to reveal the general principles and microscopic scenario of crystallization in such systems at large time and length scales. It covers both primary and secondary nucleation as well as crystallites' merging. The parameters of the DPD model were chosen appropriately to reproduce the entanglements of polymer chains. We started from an initial homogeneous disordered solution of Gaussian chains and observed the initial stages of crystallization process caused in our model by orientational ordering of polymer chains and polymer–solvent phase separation. We found that the overall crystalline fraction at the end of the crystallization process decreases with the increasing polymer volume fraction while the steady-state crystallization speed at later stages does not depend on the polymer volume fraction. The average crystallite size has a maximal value in the systems with a polymer volume fraction from 0.7 to 0.95. In our model, these polymer concentrations represent an optimal value in the sense of balance between the amount of polymer material available to increase the crystallite size and chain entanglements, that prevent crystallites' growth and merging. On large time scales, our model allows us to observe lamellar thickening linear in logarithmic time scale.

1 Introduction

Crystallization of polymer materials influences strongly their macroscopic properties and plays an important role in many applications. Understanding the microscopic mechanisms of crystallization in particular semi-crystalline polymers represents one of the most challenging unsolved problems in modern polymer physics.[1–3] From the microscopic point of view, the main difference between polymer crystallization and low-molecular inorganic crystallization results in constraining monomers by connecting them in chains. The concepts of polymer chain conformation and "chain folding"[1–3] become important. In the polymer system, long non-phantom chains form a network of entanglements, and this fact dramatically slows down the dynamics[4] and makes impossible the complete crystallization in systems with long polymer chains, so that polymers which are able to crystallize always remain semi-crystalline.[1–3]

Polymer crystallization includes many different aspects: one should distinguish crystallization from solutions and melts,

primary and secondary nucleation processes, homogeneous *vs.* heterogeneous nucleation, consider evidence for nucleation-and-growth and spinodal decomposition scenarios on different time scales, the possible presence of "precursors" (preordered mesomorphic structures and maybe even a mesomorphic phase), take into account the influence of the chain length and supercooling value, *etc.*[1–3]

Crystallization belongs to the 1st order phase transitions. One should not expect a uniform description of the crystallization process for all crystallizable polymers. However, there are universal properties of all polymer systems – connectivity of monomer units in chains, intrachain stiffness, topology (entanglements) – and therefore one could expect some general features (*i.e.*, some similarity) in the crystallization behavior of particular classes of polymers. Such general features could be, *e.g.*, a particular scenario of crystallization, initial spontaneous thickness of a lamella, its dependence on temperature, lamellar thickening with time, *etc.*[1–3]

We note here only a few open problems in understanding the crystallization of polymers. For a process from solution, the dependence of mechanisms and properties on molecular weight and on polymer concentration is still partially understood and various explanations coexist.[3,5] For early stages of polymer crystallization (both from solutions and from melts), the nucleation and growth (NG) scenario is generally considered as being realized in most polymer systems, and some mesomorphic preordered

ᵃ Faculty of Physics, Lomonosov Moscow State University, 119991 Moscow, Russia.
E-mail: kos@polly.phys.msu.ru
ᵇ Institute of Physics, Martin Luther University, 06099 Halle (Saale), Germany
ᶜ N.N. Semenov Federal research center for Chemical Physics RAS, 119991 Moscow, Russia
† Electronic supplementary information (ESI) available. See DOI: 10.1039/d0sm01545h

structures, like "baby nuclei",[6] bundles,[7] precursor layers[8] are formed. Mechanisms of growing and merging of such nuclei are still poorly understood.[3] Moreover, there is still a confrontation in the literature regarding the dominance of various scenarios, *i.e.*, nucleation and growth (NG) *versus* spinodal decomposition (SD), at early stages of primary nucleation.[2,3,9] In the present study, we addressed these questions for a particular class of polymer systems.

Microscopic computer models can shed light on many aspects of polymer crystallization. Microscopic models can be atomistic or coarse grained (CG), depending on the aspects of the real system's behavior that need to be investigated. The advantages and disadvantages of the atomistic and computational approaches are well-known, and today, multiscale modeling is required to solve most of the problems.[10,11] Atomistic and "united atom" (UA) models are suitable to reveal the microscopic mechanisms of crystallization in a particular polymer systems, however, such models have been developed so far only for a few polymers: for polyethylene (PE), polyvinyl alcohol (PVA) and poly(vinylidene fluoride) (pVDF).[9,12–20] More rough or "larger-grain" CG models imply that one bead contains several monomer units of the polymer chain. Such models are designed to reveal general patterns of crystallization in a broad class of polymer systems, *e.g.*, in semiflexible or comb-like polymers. A common way to induce crystallization of polymers in various CG models is to increase the chain stiffness using torsion and/or bond angle potentials. It stimulates chains being packed into lamellae. CG models may be sufficient to reflect some properties of real polymers, but sometimes they cannot describe other important features: the stability of the rotator phase in the UA model of the PE,[12] while the orthorhombic phase cannot be obtained using this model.[12,21] Computer simulations of polymer crystallization using various models have been performed by several groups using molecular dynamics (MD) and Monte Carlo (MC) methods.[13–36]

The general theoretical concept of folded chains in crystallized lamellae from both solutions and melts is now well-known.[3] In computer simulations, chain folding in the course of polymer crystallization was also studied both in melts[13,17,18,26,27] and solutions.[6,14,22,23,25] Possible precursors of crystalline lamella were also studied,[8,18] as well as crystallization from solutions of different solvent quality.[35]

The folding of a polymer chain in a lamella is in some sense similar to the formation of a crumpled globule[37] during the collapse of a single chain. However, this analogy with crumpled globule conformation has not yet been raised in the literature, with the exception of our previous work.[38] Although it is closely related to the intramolecular nucleation model developed by Hu *et al.*[39–41] Folded conformations of the polymer chain were observed in the simulations (coarse-grained on the united atom level), including both adjacent and random reentry.[8,26,33,41] In most cases (with the exception of a few works[36]), folded conformations were studied for only one lamella and using some special techniques such as self-seeding, the presence of a nucleation surface and a template layer[8,26,33,41] (due to computational limitations).

In computer simulations, we observed the appearance of folds in crystallizing polymers and their distribution between different seeds of crystalline lamellae during crystallization. This process starts from the state of a homogeneous solution/melt and takes quite a long time. We are interested in large length and time scales, so we need a coarse-graining going beyond the UA level. Running ahead of the story, we observed the nucleation and growth of several lamellar seeds.

Our purpose is to reveal a general scenario of initial stages of crystallization in a particular class of polymers (long semiflexible chains) under particular conditions (poor-solvent solutions, *i.e.*, fast precipitation accompanied by crystallization). Studying the crystallization scenario means studying both the primary and secondary nucleation, both the structure and size of crystallites as well as conformational properties of single chains, *i.e.*, we need large length and time scales. What such a CG model (beyond UA level) should take into account? It should definitely take into account the steric repulsion between CG beads (excluded volume interactions) and the intramolecular stiffness, while a particular choice of intermonomer attraction is not crucial for our goals (van der Waals interactions or specific interactions like, *e.g.*, hydrogen bonds). These assumptions are based on the general understanding of crystallization mechanisms in UA models of PE and PVA,[8,27,28,31,33] intermonomer attraction plays the major role only at later stages of crystallization. During initial stages of crystallization the orientational (nematic) ordering[42,43] of chain segments plays the most important role due to the excluded volume effect. It leads to chain extension and an increase of local concentration, and finally to crystallization.[33]

We used a coarse-grained model and the dissipative particle dynamics (DPD) technique[44,45] for the simulation of polymer crystallization in poor-solvent solutions and melts of semiflexible polymers. Soft potential in the DPD scheme allows the increase of the integration time step and also the decrease of the relaxation times, and these two factors make DPD in general faster than the standard MD scheme for studies of condensed polymer materials on large time scales. The DPD method is well suited for studying the equilibrium properties such as, *e.g.*, microphase separation of block-copolymers.[45–47] Due to the softness of the potentials used, there are no explicit restrictions on the value of the repulsive potential, which can make the chains partially phantom. The set of DPD parameters from the original paper[44] is not suitable to study crystallization; they are too soft. But one can choose DPD parameters to keep chains non-phantom[48] and at the same time uses the large integration step. Using our DPD model we were able to study quite large systems for long times and observe the nucleation and growth of multiple crystallites (lamellae).

We performed DPD computer simulation of poor-solvent solutions and melts of semiflexible polymers. Chain stiffness is introduced by applying stiff spring potential on bonds between beads successive along the chain, like in the tangent hard spheres model.[49] This potential can reestablish steric interactions even in the model with soft-core repulsion potential. It stimulates chain segments to undergo liquid crystalline (nematic) transition[42,43] which is the first stage of crystallization in our systems. Connectivity of monomer beads in chains, intrachain stiffness and topological restrictions (entanglements of non-phantom

chains) are the three "whales" on whom the crystallization behavior in our model "rests". Although individual features of the crystallization process in a specific polymer can be different, we believe that general trends and several common regularities of the melt and poor-solvent solution crystallization process should be the same for all semiflexible polymers, and our model is able to grasp the essence of this process. Our model is closely related to the crystallization of semiflexible polymers caused by their fast precipitation from a poor-solvent solution[35,50] accompanied by orientational ordering of chains, which is typical for many polymer processing schemes, including fiber formation.[51] In this study, we tried to reveal some general features and molecular mechanisms of crystallization in solutions and melts of semiflexible polymers, which do not depend on the polymer chemical structure, but are associated with the universal polymer properties, chain connectivity, stiffness and entanglements.

This paper is organized in a traditional way: we start with the description of our model and simulation techniques, then present our results and finish with conclusions.

2 Simulation methodology

DPD is a method of a coarse-grained molecular dynamics with a stochastic DPD thermostat conserving total momentum and angular momentum and with soft potentials mapped onto the classical lattice Flory–Huggins theory.[44,45] Macromolecules are represented in terms of the bead-spring model, with particles of equal mass (chosen to be the mass unity) and equal size. One polymer bead in our model resembles a part of a polymer chain consisting of several monomer units, and one bead of a solvent includes several solvent molecules. Beads are interacting by pairwise conservative force, dissipative force and random force:

$$f_i = \sum_{i \neq j} (F_{ij}^b + F_{ij}^c + F_{ij}^d + F_{ij}^r), \qquad (1)$$

where f_i is the force acting on the i-th bead, and the summation is performed over all neighboring beads within the cut-off radius r_c, which is chosen to be the length unity, $r_c = 1$. The first two terms in the sum are conservative forces. The term F_{ij}^b is the spring force describing the chain connectivity of beads:

$$F_{ij}^b = -k(r_{ij} - l_0)\frac{\mathbf{r}_{ij}}{r_{ij}}, \qquad (2)$$

where $\mathbf{r}_{ij} = \mathbf{r}_j - \mathbf{r}_i$, $\mathbf{r}_i$ is the coordinate of the i-th bead, $r_{ij} = |\mathbf{r}_{ij}|$, k is the bond stiffness parameter, and l_0 is the equilibrium bond length. If beads i and j are not connected by bonds, $F_{ij}^b = 0$. The term F_{ij}^c is the soft core repulsion between beads i and j:

$$F_{ij}^c = \begin{cases} a_{ij}(r_c - r_{ij})\mathbf{r}_{ij}/r_{ij}, & r_{ij} \leq r_c \\ 0, & r_{ij} > r_c \end{cases}, \qquad (3)$$

where $r_c \equiv 1$, a_{ij} is the maximal repulsion force between beads i and j for $r_{ij} = 0$. This repulsion force acts also between beads connected by bonds. Since F_{ij}^c has no singularity at zero distance, a much larger time step than in the standard molecular dynamics can be used without loosing the stability of a

numerical scheme for integrating the equations of motion, and this makes it possible to access larger time scales when complex polymeric systems are studied.[44,45] Other constituents of f_i are random force F_{ij}^r and dissipative force F_{ij}^d acting as a heat source and the surrounding media friction, respectively.[44] The parameters for these forces are: noise parameter $\sigma = 3$, friction force parameter $\gamma = 4.5$. More detailed description of our simulation methodology can be found elsewhere.[46,47]

We study systems with different polymer volume fractions $\varphi = 0.2, 0.5, 0.7, 0.8, 0.9, 0.95$ and 1.0. This total polymer volume fraction is constant during the simulation, but the local polymer concentration can change significantly. Since the DPD scheme uses explicit solvent particles, for systems with $\varphi < 1$ the rest of simulation box is filled by solvent beads. We performed simulations at constant density and constant temperature (in our simulations $k_BT = 1$). The total number density of DPD particles in our systems was $\rho = 3$ (in units of r_c^{-3}). The repulsion parameter between polymer and solvent particles, $a_{ps} = 160$, was chosen to be larger than polymer–polymer interaction parameter, $a_{pp} = 150$. Their difference equals $\Delta a = a_{ps} - a_{pp} = 10$. Such a condition corresponds to a poor solvent case, and the Flory–Huggins parameter of the polymer–solvent interaction can be calculated as $\chi_{ps} = 0.306\Delta a$ (see ref. 44) and occurs to be $\chi_{ps} \approx 3$. This mimics the situation of a fast polymer precipitation from solution with simultaneous crystallization, which is typical for many polymer processing schemes, including fiber formation.[51]

The use of soft volume and bond potentials leads to the fact that the chains are formally "phantom", i.e., their self-crossing can happen in three dimensions. The phantom nature of chains can significantly affect the dynamic properties of the system. Chain "phantomness" greatly speeds up the equilibration of the system. As regards the dynamic properties, it was shown that the original DPD method is consistent with the Rouse dynamics[52,53] which is relevant only for ideal polymers and non-entangled polymer melts. When studying the crystallization behavior, explicit entanglements between chains due to steric interactions require consideration. One should introduce some additional forces that forbid the self-intersection of the chains. These forces are usually quite cumbersome and slow down the computation significantly. Several methods were developed to avoid the bond crossings in CG models (see, e.g., the review[11]). Nikunen et al.[48] described a method for keeping chains to be non-phantom in DPD simulations without any additional forces. We used this quite simple and fast method[48] which has been proven to reproduce entanglements and polymer reptational dynamics reasonably well.[38,45,48,54] This method is based on geometrical considerations (Fig. 1). When the distance between any two non-bonded beads is greater than r_{min}, every bead in the system effectively has an excluded volume with radius $r_{min}/2$. Then, the chains are non-phantom if the condition $\sqrt{2}r_{min} > l_{max}$ is satisfied at every step during the simulations,[48] where l_{max} is the maximum bond length. Despite the fact that particles in DPD are formally point-like objects, they have an excluded volume due to the presence of repulsive potential determined by the value of a_{ij}, eqn (3).
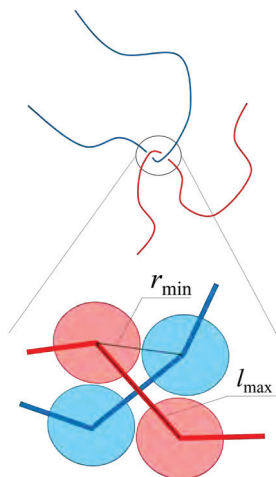
Fig. 1 Schematic representation of two chains to check bond crossing conditions.

In this study, we used $a_{pp} = a_{ss} = 150$, $a_{ps} = 160$, $l_0 = 0.2$, and $k = 150$, so the probability of chain intersection events is negligibly small, see Fig. S1 in ESI.† The big value of repulsion parameter $a_{pp} = a_{ss} = 150$ and the integration time step determine the smallest possible distance between particles. The small value of equilibrium bond length $l_0 = 0.2$ together with stiff spring potential $k = 150$ brings bonded beads closer to each other than non-bonded ones. When the chain crossing events are rare, the entanglement behavior still persists in polymer melts.[55]

Repulsive volume interactions between beads i and $i \pm 2$, $i \pm 3 \ldots$ provide an effective chain stiffness, similar to the tangent hard sphere model.[49] A large value of bond stiffness $k = 140$ as well as a small value of initial bond length $l_0 = 0.2$ contribute to the effective chain stiffness. We can still use a fairly large integration time step $\Delta t = 0.02$.

Solutions of self-avoiding semiflexible chains demonstrate a tendency to undergo lyotropic nematic ordering transition[42,43] at high polymer concentrations only due to steric interactions. This orientational ordering is often the first stage of a possible crystallization transition.[33,34,56] The obtained average distance between bonded monomer units is $\langle l \rangle = 0.48$ (in units of r_c), the chain persistence length b is about 2.3 monomer units, i.e., $\tilde{b} = b \cdot \langle l \rangle = 1.1$ in units of r_c, as we have estimated using the bond autocorrelation analysis.[57,58] Calculation of the persistence length was performed under θ-solvent conditions, we averaged the data over 5 independent runs. Note that the intramolecular stiffness is actually rather small in our model, but additional chain stiffening (increase in the persistence length) occurs due to nematic ordering.[59]

We have used rather long chains of $N = 10^3$ beads. The initial conformation of the system was prepared as sets of Gaussian chains (random walks) with the step (bond length) $l = 0.48$ and the polymer volume fraction φ. Then, the system was filled with solvent beads until the total number density $\rho = 3$ was reached. Each system was equilibrated for 10^6 DPD steps in a θ-solvent, i.e., with the values of parameters equal to $a_{pp} = a_{ss} = a_{ps} = 150$,

$l_0 = 0.2$, and $k = 150$. At this stage of modeling, the formation of a certain structure has already started due to the chain stiffening and local orientational ordering of semi-flexible chains.[43]

Thereafter, the quality of solvent was instantly changed to poor-solvent conditions corresponding to the Flory–Huggins parameter $\chi \approx 3$, which is equivalent to a deep quenching, i.e., the value of polymer–solvent interaction parameter was set to $a_{ps} = 160$. We simulated each system for 10^8 DPD steps.

The simulation cell was defined as a cubic box with the edge size $L_{box} = 50r_c$, with periodic boundary conditions in all directions. There were totally 375 000 DPD beads in the simulation box with the maximum number of polymer chains $N_{chains}^{(max)} = 375$ at $\varphi = 1$. In the starting conformations, the average end-to-end distance of a Gaussian chain with $N = 10^3$ and $l = 0.48$ is equal to $R = l\sqrt{N} \approx 15$ (this is well seen in Fig. 7a below). After a very long equilibration of our semiflexible chain in a θ-solvent or in a melt the end-to-end distance would of course become larger, $R = 2bl\sqrt{N/2b} \approx 32.5$, which is still smaller than the box size (here we used the estimation for Kuhn segment being twice the persistence length, $l_K \approx 2\tilde{b} = 2bl$). In Fig. 7a below, although the chains swell on local scales, the average distance between chain ends in the final conformation (obtained after 10^8 DPD steps) does not change too much in the course of simulation for all systems with different polymer volume fractions and becomes only slightly larger ($R \sim 17$) in comparison with the starting Gaussian conformation. Thus, on average each polymer chain does not interact with itself via periodic boundaries, neither in the starting, nor in the final conformation, or at least possible effects from such interactions are weak. This is also true even when a percolating cluster appears in our simulation box because a percolating cluster consists of multiple chains.

We performed averaging over 5 independent simulation runs for each φ-value (the parameters related to single chain properties were averaged also over all chains in a simulation box). For the calculations, we used our own original parallelized DPD code with domain decomposition.[46,47] We checked that our implementation works about 1.8 times faster than DPD code embedded in LAMMPS.

To characterize the system morphologies, we implemented the following two-stage cluster analysis. In the first stage, we consider bonds $\boldsymbol{v}_i$ connecting two successive beads (monomer units) $i - 1$ and i (Fig. 2). Coordinates of centers of bonds are the coordinates of bonds, and directions of bonds are vectors between two successive beads. We determine which bonds belong to the crystalline fraction, and then we perform cluster analysis to find crystallites composed from these "crystalline" bonds. To recognize whether a particular bond $\boldsymbol{v}_i$ belongs to the crystalline phase we use the following rules, Fig. 2a.

1. For each bond $\boldsymbol{v}_i$, we determine all neighboring bonds $\boldsymbol{v}_j$ as bonds inside a sphere with the center at the center of bond $\boldsymbol{v}_i$ and radius $R_c = 1.5r_c$. In the system with polymer volume fraction $\varphi = 1$, each bond has ~ 18 neighbors.

2. Then, we define the number of neighboring bonds $\boldsymbol{v}_j$, which are collinear with the selected one, $\boldsymbol{v}_i$. For this goal, we calculate the angle θ_{ij} between bonds $\boldsymbol{v}_i$ and $\boldsymbol{v}_j$ and use the following collinearity threshold criteria: two bonds $\boldsymbol{v}_i$ and $\boldsymbol{v}_j$ are
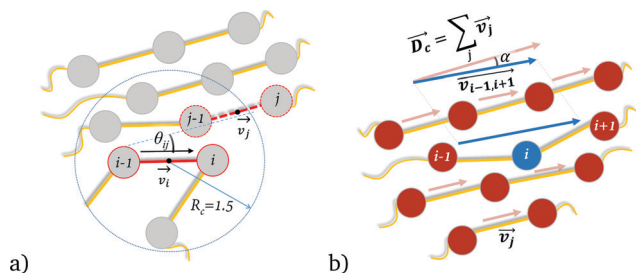
Fig. 2 Stage one: schematic illustration of the crystallinity criterion for a polymer bond (a). Stage two: schematic illustration of the crystallinity criterion for a polymer bead (b).

collinear if the angle between them is less than 17 degrees, $\theta_{ij} < 17$ degrees.

3. Finally, we calculate the ratio of the number of collinear neighbors to the total number of neighbors. Bond $\boldsymbol{v}_i$ is marked "crystalline" if this ratio is greater than 0.4, otherwise it is marked "amorphous", and this is our bond crystallinity criteria (this procedure is quite similar to the crystallinity criteria used previously in MC simulations of isotropic–nematic phase transition[60] and MD simulations of crystallization in alkanes[33]).

After such labeling, we perform the standard clustering analysis[61] using cut-off radius $R_c = 1.5r_c$ to find the clusters formed by neighboring "crystalline" bonds.

In the second stage, we turn to the consideration of the beads and mark a bead "crystalline" if it is either the beginning or the end bead of at least one crystalline bond, otherwise it is marked "amorphous". This procedure transforms the system of bonds into the system of beads. However, after the first stage some "amorphous" beads were still located inside crystalline clusters. We consider "amorphous" beads in the neighborhood to "crystalline" beads within the cutoff radius $R_c = 1.5r_c$. We define the direction of such beads (i) as the vectors between beads ($i − 1$) and ($i + 1$). Then we check the following criteria, Fig. 2b:

1. Calculate the director $\boldsymbol{D}_c$ for each cluster, *i.e.*, the unit vector corresponding to the preferred orientation of the beads in a crystallite (the normalized sum of all beads in a cluster).

2. Compare the directions of the cluster director $\boldsymbol{D}_c$ and a neighboring "amorphous" bead. If the angle α between the cluster direction and the bead direction is less than $\alpha < 20$ degrees, the bead is marked "crystalline" and added to this cluster, otherwise the bead stays "amorphous".

The first stage (bonds) is more sensitive to the local fluctuations than the second stage (beads), because the direction of a bond is the vector between i and $i + 1$ beads and the direction of a bead is the vector between $i − 1$ and $i + 1$ beads. After the first stage, crystallites contain many "amorphous" beads inside them. The DPD potential of the excluded volume is soft, which causes coordinate and direction fluctuations. The second stage of the analysis is aimed to reassign these "amorphous" beads inside crystallites to the "crystalline" beads in order to avoid artificial appearance of amorphous beads inside crystallites.

In our simulations, we looked at the average size, the number of crystallites, and the degree of crystallinity as functions of time and polymer volume fraction. To characterize polymer chain conformations, we calculated the dependence of the average squared spatial distance between two monomers on their distance along the chain, $R^2(n)$, separately for the segments belonging to crystalline and amorphous fractions, respectively. This dependence allows the analysis of the polymer structure on different length scales.[38,62] For different polymer concentrations, we also calculated the distributions of crystalline segment (stem) lengths, *i.e.*, the strongly extended parts of polymer chains inside crystallites.

3 Results and discussion

In Fig. 3, we represented the final morphologies of several systems with different polymer volume fractions φ after long equilibration time. Solvent particles are hidden, and red and blue colors represent the "crystalline" and "amorphous" beads, respectively. Solvent (transparent) or "amorphous" (blue) beads separated crystallites (red). The linear size of a typical crystallite is smaller than the simulation box size, so that a single crystallite does not interact with itself through periodic boundaries (a possible case of percolating crystallites is discussed below). Visually, the crystallite size seems to have the largest value for polymer volume fraction φ between 0.7 and 0.95.

Fig. 4 shows a more detailed view of a typical system with 0.5 polymer volume fraction at an intermediate time of 10^7 DPD steps, including its crystallization behavior and cluster structure. In Fig. 4a one can see the polymer–solvent separation as well as the separation of the polymer-rich phase into crystalline and amorphous sub-phases. The crystalline sub-phase is comprised of several crystallites (see Fig. 4b), which could be easily found by our two-stage clustering analysis described above.
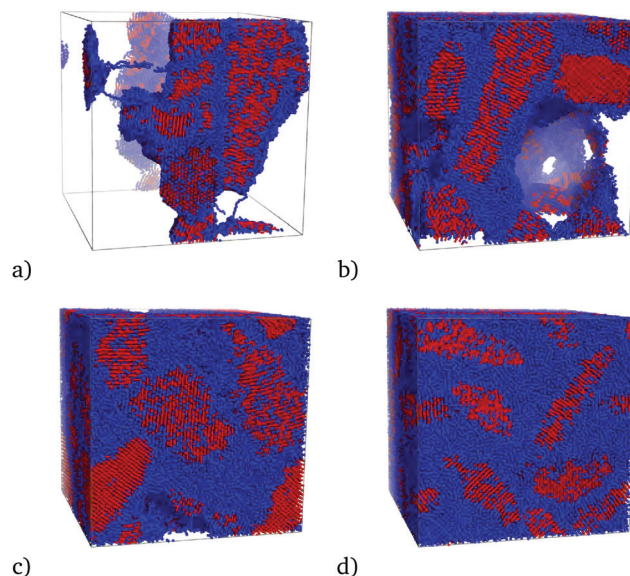

Fig. 3 Snapshots of several systems with different polymer volume fraction φ at the end of equilibration, $t = 10^8$ DPD steps: $\varphi = 0.2$ (a), $\varphi = 0.7$ (b), $\varphi = 0.9$ (c), $\varphi = 1$ (d). Only polymer beads are shown ("crystalline" beads are red and "amorphous" beads are blue), while solvent beads are hidden.
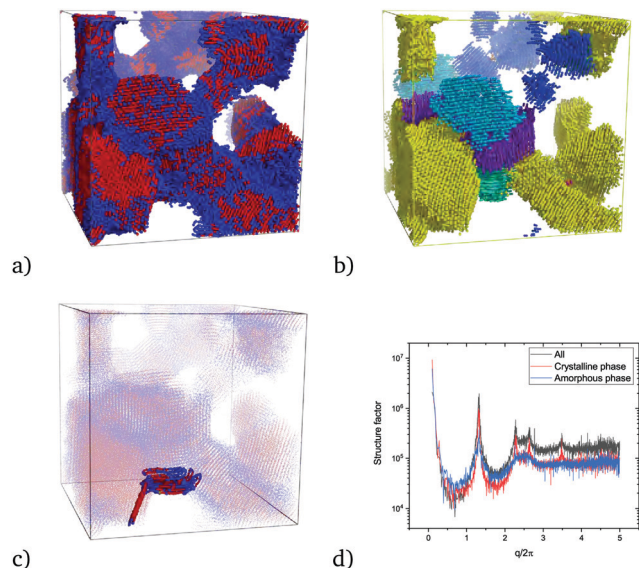
Fig. 4 (a) Snapshot of a system with 0.5 polymer volume fraction (some intermediate morphology in the course of equilibration): red beads are "crystalline" and blue beads are "amorphous", solvent beads are not shown. (b) The same system after both stages of the cluster analysis: different colors correspond to different crystalline clusters, and "amorphous" beads are not shown. (c) The conformation of a randomly chosen single polymer chain from (a). (d) The static structure factor for the polymer beads (black) and separately crystalline (red) and amorphous (blue) phases from (a).

These crystallites can have quite complex surfaces and very different sizes. Analysis of the maxima in static structure factor (see Fig. 4d) shows the ratio between peaks $1:\sqrt{(3)}:2$. Such a ratio of Bragg peaks confirms that chain parts (stems) in crystallites have hexagonal packing[18] corresponding to the rotator phase. The radial distribution functions, $G(r)$, for the whole system and for its components show that the crystalline phase is slightly more dense than amorphous one in solutions and becomes more noticeably dense in the melt, see Fig. S2 in the ESI.†

To study the crystalline structure in detail we calculated the Steinhardt bond order parameters Q_4, Q_6, W_4 and W_6[63,64] for amorphous and crystalline phases, see Fig. S3 in the ESI.† There is a very small difference between the two clouds of points in the Q_4–Q_6 and W_6–Q_6 planes, so that we cannot distinguish the amorphous and crystalline phases from these data. Actually, this is not surprising because we cannot expect a three-dimensional crystalline ordering in our system, but rather the formation of some hexagonal packing of chain stems inside lamellar crystallites like in the rotator phase. To reveal the existence of such ordering, another parameter is better suitable, namely, the parameter $\psi_6 = \left\langle \left\| \frac{1}{NN_{\text{chains}}} \sum_{i=1}^{NN_{\text{chains}}} \frac{1}{n_i} \sum_{j=1}^{n_i} \exp(i6\alpha_{ij}) \right\| \right\rangle$, where α_{ij} are the angles between the vectors connecting monomer i to its neighbors j and a fixed axis in the plane perpendicular to the director of a crystallite, and n_i is the number of neighbors of bead i within the cutoff radius (which was chosen as $1.6r_c$). This parameter was first introduced for studying 2D crystallization in

hard disk systems[65–67] and recently used for revealing hexagonal 2D packing in a model melt of semiflexible polymers encompassing a liquid and a hexagonal rotator-like crystal phase,[21] where it was found to be equal to $\psi_6 \approx 0.28$ for "liquid" (actually amorphous nematically ordered polymer melt) and $\psi_6 \approx 0.6$ for hexagonal rotator-like crystalline polymer melts.[21] We performed this analysis of rotator-like crystalline ordering, as well as the orientational nematic ordering, separately for each crystallite and for the amorphous phase.

To analyse the orientational (nematic) ordering, we calculated for every single crystallite and for amorphous phase the eigenvalues S_1, S_2, S_3 of the orientational tensor[21,33,59] for polymer bonds, $Q_{\alpha,\beta} = \frac{1}{(N-1)N_{\text{chains}}} \sum_{i=1}^{(N-1)N_{\text{chains}}} \frac{1}{2}(3e_{i\alpha}e_{i\beta} - \delta_{\alpha\beta})$, where $e_{i\alpha}$ is the α component of the unit vector along the bond i. For the ideal nematic ordering these eigenvalues are equal to $(1, -0.5, -0.5)$ and for the isotropic system they are $(0,0,0)$. In ESI,† Fig. S4, we represented the box plots for S_1, S_2, and S_3. The amorphous phase is isotropic while the crystallites show pronounced nematic ordering. In Fig. S5 in the ESI,† we have shown the dependence of the eigenvalues S_1, S_2, and S_3 on the size of crystallites. For very small clusters the nematic ordering is perfect while with increasing the cluster size, we observe crystallites with both quite small $S_1 < 0.4$ and large $S_1 > 0.8$ values. We assume that large crystallites have non-ideal shape like, e.g., bent lamellae, and this significantly affects the eigenvalues of orientational tensor leading to decreasing of S_1, although there are also large crystallites with very high nematic ordering.

We plotted the distributions (box plots) of parameter ψ_6 for crystallites and amorphous phase in Fig. S6 in the ESI.† The results indicate proper distinguishing of crystalline and amorphous phases. In the amorphous phase the value ψ_6 is close to zero. Quite high values (more than 0.5, even above 0.7) are observed for a few crystallites, but on average these values are rather moderate – about 0.2, although widely distributed. This can be explained by two reasons: (1) the structure is not perfect and (2) most of the clusters are rather small, so that most beads in small clusters lie on their surface and do not have enough neighbors. Dependencies of ψ_6 on the crystallite size are shown in Fig. S7 in the ESI.† There is a clear trend towards increasing ψ_6 with increasing cluster size, although the width of the distribution also grows, so that there are also small values of $\psi_6 < 0.1$ for clusters larger than 10 000 beads. The dependencies of ψ_6 on the first eigenvalue S_1 do not demonstrate a clear correlation between these two parameters, see Fig. S8 in the ESI.† However, high values $\psi_6 > 0.3$ are observed for clusters with S_1 between 0.4 and 0.95, and the "record" is $(\psi_6, S_1) = (0.7, 0.7)$.

A single chain may contribute to several crystallites (e.g., the chain shown in Fig. 4c is involved in two different crystallites). In general, the crystallite structure is similar to that obtained, e.g., for another model by means of MD simulation.[18] Thus, a preliminary conclusion here is that our model and the DPD simulation scheme keep the chains to be non-phantom (which is crucial for polymer crystallization), reproduce reasonably

good some general features and are suitable for studying the crystallization in polymers on quite large length scales.

Fig. 5 and 6 present the physical quantities which are the main characteristics of the crystalline sub-phase – the average size of crystallites (in beads), the normalized number of
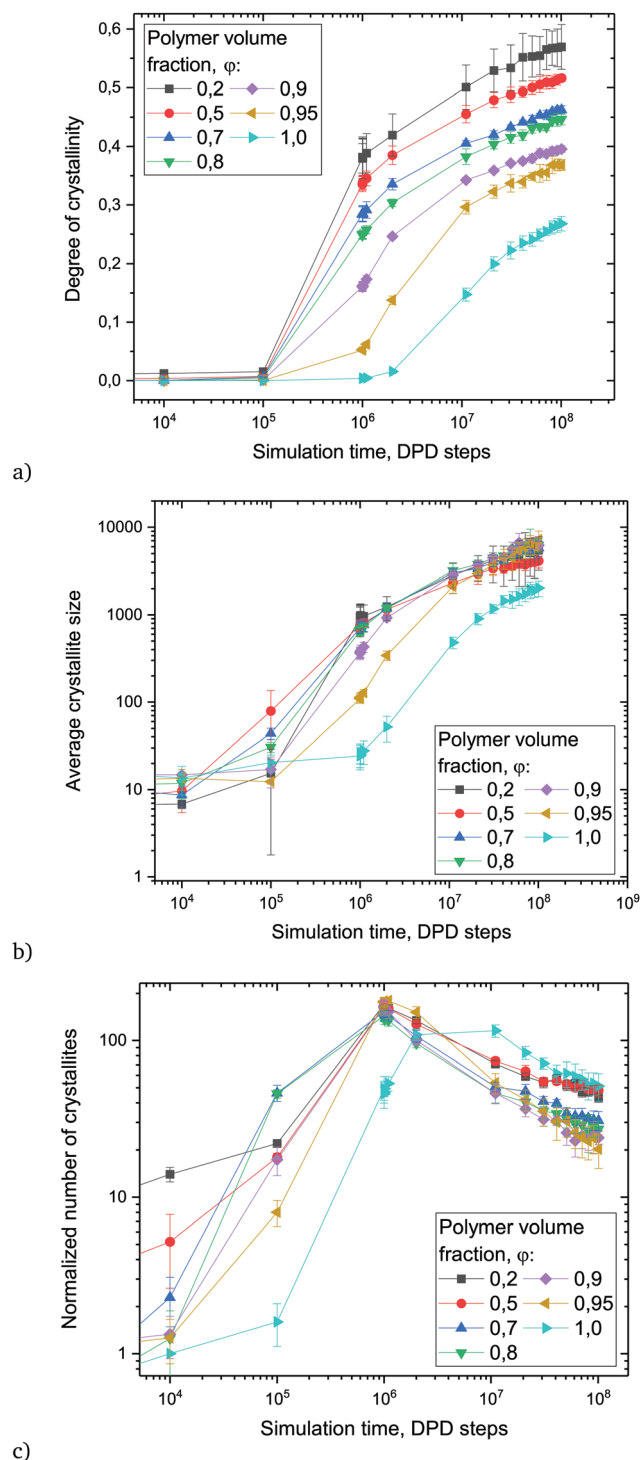

Fig. 5 Time dependencies of the degree of crystallinity (a), of the average crystallite size (b), and of the normalized number of crystallites (c) for systems with different polymer volume fractions (shown in the legend).
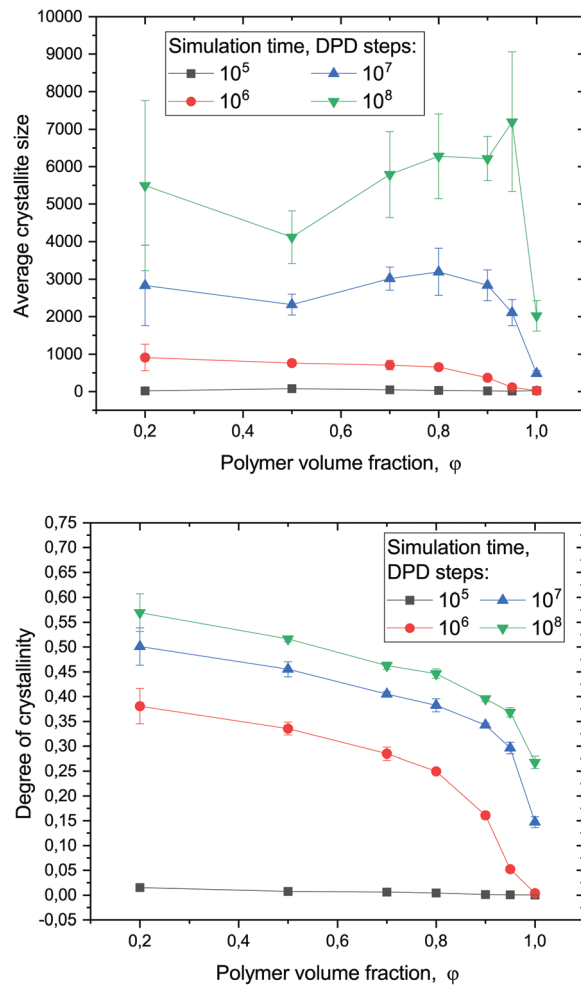

Fig. 6 Dependence of the average crystallite size (a) and the degree of crystallinity (b) on polymer volume fraction at different times (in DPD steps, shown in the legend) during the crystallization process.

crystallites (*i.e.*, the number of crystallites divided by the polymer volume fraction φ), and the degree of crystallinity (*i.e.*, the number of crystalline beads divided by the total number of polymer beads) – at different times and for different polymer volume fractions. We indicated error bars in these figures to confirm the validity of our results. We used lines connecting the data points without any smoothing as an eye guide.

In Fig. 5a one can observe the process of crystallization on a logarithmic timescale – the degree of crystallinity starts to increase quite rapidly after about 10^5 DPD time steps for small polymer volume fractions φ and after about 10^6 DPD time steps for large polymer volume fractions φ. The time when this initial growth of the degree of crystallinity has a maximal slope coincides with our estimation for the local crystallization time τ, which we defined from Fig. 5c as the time of formation of maximal number of crystallites. This time τ depends on φ due to the preliminary orientational ordering in good solvent and different speeds of the polymer–solvent separation after quenching. After this initial relatively rapid increase of the

degree of crystallinity, a steady-state regime of logarithmically slow crystallization process starts at times about 10^7 DPD time steps. The kinetic reason for this slowing-down is the network of entanglements in the concentrated polymer solution (or even melt after separation from the solvent), so that the full relaxation time for such a system is expected to be comparable with reptation time,[4] *i.e.*, being of the order τN^3. Because in our simulations the polymer length is $N = 10^3$, there is no hope to reach a true thermodynamic equilibrium in such systems, both in simulations and in real experiments (crystallizable polymers always stay semi-crystalline), and we can only discuss the properties of some quasi-equilibrium steady-state systems with slow evolution toward morphologies with a higher degree of crystallinity. The sigmoidal shape of this curve is typical for the nucleation and growth scenario. However, in our model, we observed interesting features: the crystallization speed is almost the same with good accuracy in the steady-state regime for systems with φ from 0.2 to 0.95. This is probably because the entanglement length N_e is similar for those polymer systems (see Fig. S9 in the ESI† for time evolution of N_e).

The calculation of N_e was carried out in a similar manner to the procedure developed by M. Kröger's group[68–71] (this method gives an average value of N_e for all chains in a system). In our simulations, we did not observe a considerable increase of N_e during the whole simulation time (except the very short time in the beginning). This observation is consistent with the argument for a long reptation time given above. The entanglement length increases (*i.e.*, the chains become less entangled) quite fast only in the beginning of simulations, and afterwards it stays almost constant for all systems. In the initial configurations, the entanglement length is $N_e \approx 10$ for $\varphi = 1$ and 0.9 and $N_e \approx 70$ for $\varphi = 0.5$. During the first 100 DPD steps it increases to $N_e \approx 30$ for $\varphi = 1$, $N_e \approx 40$ for $\varphi = 0.9$ and $N_e \approx 200$ for $\varphi = 0.5$. At the end of simulation (10^8 DPD steps), N_e becomes slightly bigger in concentrated systems and almost does not change in dilute systems: $N_e \approx 40$ for $\varphi = 1$, $N_e \approx 60$ for $\varphi = 0.9$ and $N_e \approx 200$ for $\varphi = 0.5$. This procedure for analysis of entanglement length was already used previously in studies of polymer crystallization.[31,32,72]

The time evolution of the average crystallite size (measured in beads) shows a rather fast growth on times between 10^5 and 10^6 DPD steps and much more slow growth on larger times (Fig. 5b). Interestingly, the largest average cluster size is achieved for polymer volume fraction in the range $\varphi \in [0.7, 0.95]$ (see more discussion below). The data for average cluster size (used in Fig. 5b and in Fig. 6a below) were obtained using the cluster size distribution shown in Fig. 7b below (with a minimal crystallite size cutoff equal to 5 beads in order to avoid contribution of small crystallites).

Fig. 5c shows the total number of determined crystallites divided by the polymer volume fraction φ and gives more insight into the crystallization process. On small times, we observed a sharp increase of the number of crystallites. One can see a well-defined maximum (local crystallization time τ) around 10^6 DPD steps for all systems in solutions and around 10^7 DPD steps for the melt. A pronounced decrease of the number of crystallites is consistent with the fast growth of
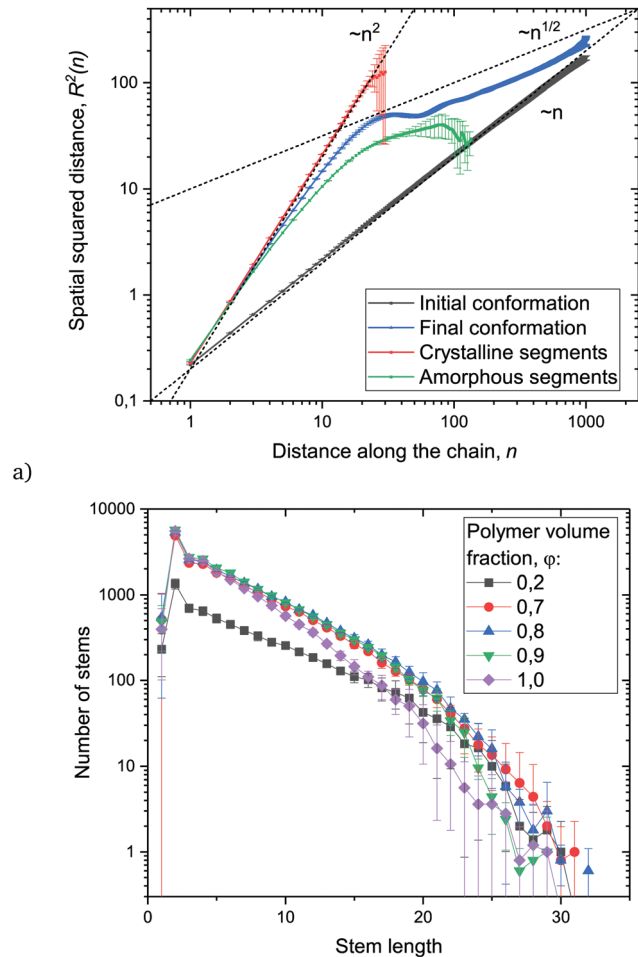

a)

b)

Fig. 7 Squared spatial distance R^2 between two beads *versus* distance n between them along the chain for initial (black line) and final (blue curve) conformations of a system with polymer volume fraction $\varphi = 0.9$ (a). For the final conformation, dependencies $R^2(n)$ are plotted also separately for crystalline (red curve) and amorphous (green curve) segments (a). Distribution of length of crystalline segments (stems) in systems with different polymer volume fraction (shown in the legend) at the end of simulations at time 10^8 DPD steps (b).

average crystallite size. The initial increase represents the nucleation process, when many small crystallites (crystalline seeds) are formed in the system, and this stage of crystallization starts to saturate at the time moment when the overall degree of crystallinity starts to increase, Fig. 5a. After that moment the number of crystallites starts to decrease both due to the process of merging of small crystallites into larger ones and due to adding new chain stems from amorphous sub-phase to crystallites (secondary nucleation or growth of crystallites). Merging of small crystallites occurs most probably due to filling the space between two crystallites by new chain stems from amorphous phase which become crystalline but not due to diffusion of crystallites towards each other. More interestingly, during this second regime all systems have very similar behavior, and we suspect even the existence of a universal power-law decrease of the number of crystallites at late stages of crystallization while the slope of this decrease is maximal for systems with a

polymer volume fraction in the range $\varphi \in [0.7, 0.95]$, *i.e.*, in concentrated solutions. To summarize, at the late stages of the observed crystallization process (after 10^7 DPD steps) the degree of crystallinity and the average size of crystallites increase while the number of crystallites decreases.

The length and time scales available in our simulations allow the observation of many crystallite seeds in the simulation box and their growth and merging. In the movie of the system evolution (see Fig. S10 and movie in the ESI†), we observed both the addition of chain stems to the lateral faces of growing crystallites and the diffusion of chain parts inside crystallites through their end faces, as it was also observed previously in MD simulations of UA models.[8,27,33,34]

In Fig. 6, we observed that the average crystallite size (in beads) is maximal at intermediate values of the polymer volume fraction $\varphi \in [0.7, 0.95]$ at large time scales, while the degree of crystallinity is monotonically decreasing with increasing φ at all times. This feature originates from the competition of two opposite processes that limit the crystallite growth: (i) at small concentrations there is a lack of the surrounding polymer material, while (ii) at high concentrations the entanglement effect from surrounding chains is so strong that it prevents the segment diffusion on large distances as well as the local orientational rearrangement of polymer segments in amorphous regions (these are two processes, which are necessary for merging of small crystallites into larger ones).

In order to understand the structure of crystallites, we studied the conformations of chain segments inside and outside crystallites. In Fig. 7a, we plotted the average squared spatial distance R^2 between two monomer units *versus* the distance n between them along the chain for the system configurations in the beginning and at the end of simulation. Although we presented the data for the system with $\varphi = 0.9$ polymer, the systems with another polymer volume fraction demonstrated similar behavior. The initial starting conformation of all chains in the system was Gaussian, so that the corresponding dependence lies exactly along the line $R^2(n) = l^2 n$ (black line), where l is the bond length.

The data for the conformations at the final time of simulation (10^8 DPD steps) are shown for the entire chains (blue curve) as well as separately for crystalline (red curve) and amorphous (green curve) segments. It is clear that the crystalline stems have rod-like conformations, and this leads to the power law dependence $R^2(n) \sim n^2$. Contrary to that, chain parts consisting of amorphous segments have quite extended conformations only on small length scales along the chain, while on large scales they look like very compact conformations. Crystalline segments have quite short length (not larger than 30 beads) while the amorphous segments can reach the length of about 200 beads. The dependence for entire chains (blue curve), after the steep increasing $R^2 \sim n^2$ shows a plateau starting at $n \sim 30$ (which is approximately the stem length) and ending at $n \sim 60$ (which is approximately two stem lengths), while the scaling on large distances along the chain ($n > 60 \approx N_e$) is $R^2 \sim n^{1/2}$, *i.e.*, $R \sim n^{1/4}$. On the scale of the whole chain ($n \approx 1000$) the end-to-end distance does not change too much:

for the initial Gaussian conformation before crystallization, $R^2(1000) \approx 180$, and for the final one, $R^2(1000) \approx 250$.

The observed $R \sim n^{1/4}$ scaling means effectively "more strongly crumpled" conformations on the scales larger than the stem segment size in a crystallite, in comparison to the scaling for a single usual crumpled (fractal) globule.[37] Scaling $R \sim n^{1/4}$ was first reported for lattice animals[73] and can also mean effectively more dense packing of some interpenetrating objects like soft spheres or Gaussian blobs. In our systems, we have the case of more dense packing of hairpins from different chains (or from the same chain but separated from each other along the chain) in a single dense crystalline lamella. Hairpins could be packed more densely than their linear size assumes. We checked the distribution of the degree of crystallinity along the chain for the systems with 50 and 100% polymer volume fractions, see Fig. S11 in the ESI.† We observed significant peaks at the chain ends, showing that the end monomer units (about 3 units) have higher chance to be amorphous (due to higher entropy) and the few next monomer units (about 5–15 units) have higher chance to be a part of a crystallite. The large central part of the dependence has a plateau with the value corresponding to the average degree of crystallinity.

The final distributions of the length of crystallized segments (stems) for different polymer volume fractions are presented in Fig. 7b. We observed the exponential Flory-like distribution of segment lengths (for stems shorter than 20 beads), and these curves look very similar for all studied systems, especially for concentrated solutions with polymer volume fractions $\varphi \in [0.7, 0.9]$. We can conclude from this plot that the internal structure of all crystallites is actually the same for all systems under study, with approximately the same maximal lamella thickness around 25–30 monomer units.

In Fig. 8, we plotted the time dependence of the average stem length at large time scales. The average was calculated over the distribution shown in Fig. 7b and over the similar distributions
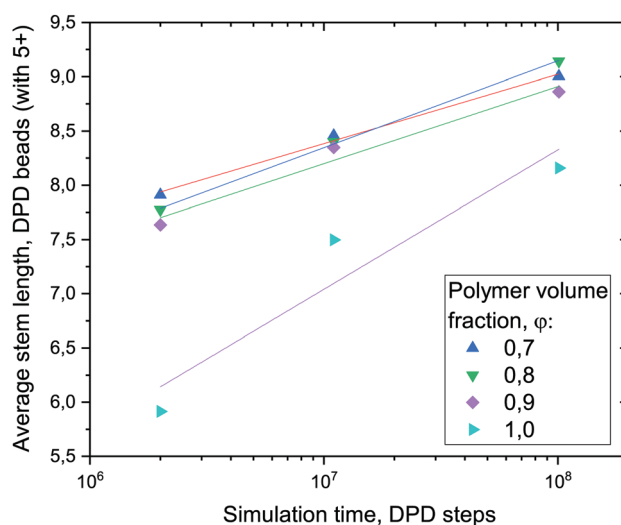

Fig. 8 Dependence of the average stem length on time for systems with different polymer volume fractions (shown in the legend).

calculated at time moments 2×10^6 and 10^7 DPD steps. For the averaging over distributions we chose the stem size equal to 5 as the left bound of the averaging interval. In Fig. 8, we see crystalline lamellar thickening in logarithmic time scale.[1–3]

4 Conclusions

In this study, we performed coarse-grained DPD computer simulations of the crystallization process of long semiflexible polymer chains (of the length $N = 1000$ monomer units) in melts and solutions with various polymer volume fractions and under poor solvent conditions, which is typical for many polymer processing schemes.[51]

For this particular process we revealed several general features (discussed below) which do not depend on the chemical structure but arise due to universal polymer properties like chain connectivity, intrachain stiffness and topology/entanglements.

Our coarse-grained DPD model appropriately modified by a (tangent-hard-spheres-like) stiffness potential resembles a wide class of semiflexible polymers in solutions and melts and is suitable to study general aspects of crystallization in polymers. We start with a randomly prepared homogeneous configuration and monitor the crystallization process for a reasonably long time reaching the later stages of crystallization such as lamellar thickening. We represent the dependencies of several observable values on the polymer volume fraction φ because this parameter governs the role of entanglements, *e.g.*, the lamellar thickness depends on φ. Parameters of the model are chosen in such a way that the pure polymeric melt ($\varphi = 1$) crystallizes (due to the steric interactions and intrachain stiffness). In solutions ($\varphi < 1$), the orientational ordering of chains and polymer–solvent separation on local scales (demixing) occur very fast, and this induces subsequent crystallization (like it was also observed in similar models for very dilute solutions[35]).

We have found that the microscopic mechanism of initial stages of crystallization in concentrated solutions of semiflexible polymers with poor solvent involves the orientational ordering of polymer chains accompanied by simultaneous polymer–solvent separation.

We have observed the two-stage (nucleation and growth) scenario of crystallization for all systems with different polymer volume fraction φ. In the first stage, the precursors of crystallites (seeds) are formed. At the end of this stage, the number of crystallites reaches its maximal value, and simultaneously a steep increase of the degree of crystallinity is observed (coincidence of time of these two events is a quite promising result). In the second stage, the initial crystallites grow and merge into larger crystallites, and this is observed as a much more slow steady-state process. This process on a large time scale is characterized by the same logarithmic time dependence of the degree of crystallinity for polymer volume fractions $\varphi > 0.5$. Merging of crystallites occurs mostly also due to crystallite growth which leads to filling the space (gap) between two crystallites by parts of chains from amorphous regions which become new crystalline stems, *i.e.*, intermediate amorphous regions became crystalline.

The overall degree of crystallinity at the end of simulation decreases with increasing the polymer volume fraction in the system. There is a non-monotonous dependence of the average crystallite size on the polymer volume fraction φ. We suppose that $\varphi \in [0.7, 0.95]$ is the optimal polymer volume fraction in a sense of balance between the available polymer material to build crystallites and chain entanglements preventing from crystallite growth and merging.

A lamella consists of many rod-like stems with a size of about 20–30 monomer units, and they are hexagonally packed. We observed logarithmic law of lamellar thickening. Each crystallite (lamella) can consist of different chains and each chain can participate in several crystallites (lamellae). Primary nucleation happens on very short time scales; we have not studied it in detail and it will be the topic of further research.

Finally, we would like to make a few more remarks. Some of our results are not new and just confirm that our model is suitable to study polymer crystallization. But, all our conclusions on the dependence of different parameters of crystallites (their size, number, length distribution of stems) on the polymer volume fraction are new and bring physical insights into polymer crystallization in poor solvent solutions of semiflexible polymers.

Conflicts of interest

There are no conflicts to declare.

Acknowledgements

References

1 *Progress in Understanding of Polymer Crystallization*, ed. G. Reiter and G. R. Strobl, Springer-Verlag, Berlin Heidelberg, 2007.
2 M. Muthukumar, *Adv. Chem. Phys.*, 2004, **128**, 1–64.
3 M. C. Zhang, B.-H. Guo and J. Xu, *Crystals*, 2017, **7**, 4.
4 M. Doi and S. F. Edwards, *The Theory of Polymer Dynamics*, Clarendon Press, Oxford, 1988.
5 A. Kundagrami and M. Muthukumar, *J. Chem. Phys.*, 2007, **126**, 144901.
6 M. Muthukumar, *Philos. Trans. R. Soc., A*, 2003, **361**, 539–556.

7 G. Allegra and S. Meille, *Phys. Chem. Chem. Phys.*, 1999, **1**, 5179–5188.

8 C. Luo and J. U. Sommer, *Macromolecules*, 2011, **44**, 1523–1529.

9 R. H. Gee, N. Lacevic and L. E. Fried, *Nat. Mater.*, 2006, **5**, 39–43.

10 J. A. Elliott, *Int. Mater. Rev.*, 2011, **56**, 207–225.

11 A. Gooneie, S. Schuschnigg and C. Holzer, *Polymers*, 2017, **9**, 16.

12 W. Paul, D. Y. Yoon and G. D. Smith, *J. Chem. Phys.*, 1995, **103**, 1702–1709.

13 T. Yamamoto, *J. Chem. Phys.*, 1997, **107**, 2653–2663.

14 T. Yamamoto, *J. Chem. Phys.*, 1998, **109**, 4638–4645.

15 N. Waheed, M. S. Lavine and G. C. Rutledge, *J. Chem. Phys.*, 2002, **116**, 2301–2309.

16 M. J. Ko, N. Waheed, M. S. Lavine and G. C. Rutledge, *J. Chem. Phys.*, 2004, **121**, 2823–2832.

17 H. Meyer and F. Müller-Plathe, *J. Chem. Phys.*, 2001, **115**, 7807–7810.

18 H. Meyer and F. Müller-Plathe, *Macromolecules*, 2002, **35**, 1241–1252.

19 T. Vettorel and H. Meyer, *J. Chem. Theory Comput.*, 2006, **2**, 616–629.

20 T. Vettorel, H. Meyer, J. Baschnagel and M. Fuchs, *Phys. Rev. E: Stat., Nonlinear, Soft Matter Phys.*, 2007, **75**, 1–14.

21 T. Shakirov and W. Paul, *Phys. Rev. E*, 2018, **97**, 042501.

22 C. Liu and M. Muthukumar, *J. Chem. Phys.*, 1998, **109**, 2536–2542.

23 P. Welch and M. Muthukumar, *Phys. Rev. Lett.*, 2001, **87**, 218302.

24 M. Muthukumar, *Adv. Polym. Sci.*, 2005, **191**, 241–274.

25 J. Zhang and M. Muthukumar, *J. Chem. Phys.*, 2007, **126**, 234904.

26 T. Yamamoto, *J. Chem. Phys.*, 2008, **129**, 184903.

27 T. Yamamoto, *J. Chem. Phys.*, 2013, **139**, 054903.

28 P. Yi, C. R. Locker and G. C. Rutledge, *Macromolecules*, 2013, **46**, 4723–4733.

29 I.-C. Yeh, J. W. Andzelm and G. C. Rutledge, *Macromolecules*, 2015, **48**, 4228–4239.

30 A. Bourque, C. R. Locker and G. C. Rutledge, *Macromolecules*, 2016, **49**, 3619–3629.

31 C. Luo and J. U. Sommer, *Phys. Rev. Lett.*, 2014, **112**, 195702.

32 C. Luo, M. Kröger and J.-U. Sommer, *Macromolecules*, 2016, **49**, 9017–9025.

33 M. Anwar, F. Turci and T. Schilling, *J. Chem. Phys.*, 2013, **139**, 214904.

34 M. Anwar and T. Schilling, *Polymer*, 2015, **76**, 307–312.

35 M.-X. Wang, *Phys. Lett. A*, 2015, **379**, 2761–2765.

36 J. Morthomas, C. Fusco, Z. Zhai, O. Lame and M. Perez, *Phys. Rev. E*, 2017, **96**, 052502.

37 A. Y. Grosberg, S. K. Nechaev and E. I. Shakhnovich, *J. Phys.*, 1988, **49**, 2095–2100.

38 A. Chertovich and P. Kos, *J. Chem. Phys.*, 2014, **141**, 134903.

39 W. Hu, D. Frenkel and V. B. F. Mathot, *Macromolecules*, 2003, **36**, 8178–8183.

40 W. Hu and D. Frenkel, *J. Phys. Chem. B*, 2006, **110**, 3734–3737.

41 W. Hu and T. Cai, *Macromolecules*, 2008, **41**, 2049–2061.

42 L. Onsager, *Ann. N. Y. Acad. Sci.*, 1949, **51**, 627–659.

43 A. Khokhlov and A. Semenov, *J. Stat. Phys.*, 1985, **38**, 161–182.

44 R. D. Groot and P. B. Warren, *J. Chem. Phys.*, 1997, **107**, 4423–4435.

45 P. Español and P. B. Warren, *J. Chem. Phys.*, 2017, **146**, 150901.

46 A. Gavrilov, Y. Kudryavtsev, P. Khalatur and A. Chertovich, *Chem. Phys. Lett.*, 2011, **503**, 277–282.

47 A. A. Gavrilov, Y. V. Kudryavtsev and A. V. Chertovich, *J. Chem. Phys.*, 2013, **139**, 224901.

48 P. Nikunen, I. Vattulainen and M. Karttunen, *Phys. Rev. E: Stat., Nonlinear, Soft Matter Phys.*, 2007, **75**, 036713.

49 C. Vega, C. McBride and L. G. MacDowell, *J. Chem. Phys.*, 2001, **115**, 4203–4211.

50 G. Raos and G. Allegra, *J. Chem. Phys.*, 1997, **107**, 6479–6490.

51 S. Eichhorn, J. Hearle, M. Jaffe and T. Kikutani, *Handbook of Textile Fibre Structure: Volume 2: Natural, Regenerated, inorganic and Specialist Fibres*, Elsevier, 2009.

52 N. Spenley, *Europhys. Lett.*, 2000, **49**, 534.

53 F. Lahmar and B. Rousseau, *Polymer*, 2007, **48**, 3584–3592.

54 A. Karatrantos, N. Clarke, R. J. Composto and K. I. Winey, *Soft Matter*, 2013, **9**, 3877–3884.

55 R. Chang and A. Yethiraj, *Macromolecules*, 2019, **52**, 2000–2006.

56 A. Markina, V. Ivanov, P. Komarov, S. Larin, J. M. Kenny and S. Lyulin, *J. Polym. Sci., Part B: Polym. Phys.*, 2017, **55**, 1254–1265.

57 R. J. Gowers, M. Linke, J. Barnoud, T. J. Reddy, M. N. Melo, S. L. Seyler, D. L. Dotson, J. Domanski, S. Buchoux and I. M. Kenney, *Proceedings of the 15th Python in Science Conference*, 2016, pp. 98–105.

58 N. Michaud-Agrawal, E. J. Denning, T. B. Woolf and O. Beckstein, *J. Comput. Chem.*, 2011, **32**, 2319–2327.

59 V. A. Ivanov, A. S. Rodionova, J. A. Martemyanova, M. R. Stukan, M. Müller, W. Paul and K. Binder, *Macromolecules*, 2014, **47**, 1206–1220.

60 A. Cuetos and M. Dijkstra, *Phys. Rev. Lett.*, 2007, **98**, 095701.

61 M. P. Allen and D. J. Tildesley, *Computer Simulation of Liquids*, Oxford University Press, 1989.

62 I. Lifshitz, A. Y. Grosberg and A. Khokhlov, *Rev. Mod. Phys.*, 1978, **50**, 683.

63 P. J. Steinhardt, D. R. Nelson and M. Ronchetti, *Phys. Rev. B: Condens. Matter Mater. Phys.*, 1983, **28**, 784.

64 W. Lechner and C. Dellago, *J. Chem. Phys.*, 2008, **129**, 114707.

65 J. Lee and K. J. Strandburg, *Phys. Rev. B: Condens. Matter Mater. Phys.*, 1992, **46**, 11190.

66 E. P. Bernard and W. Krauth, *Phys. Rev. Lett.*, 2011, **107**, 155704.

67 C. Avendano and F. A. Escobedo, *Soft Matter*, 2012, **8**, 4675–4681.

68 M. Kröger, *Comput. Phys. Commun.*, 2005, **168**, 209–232.

69 S. Shanbhag and M. Kröger, *Macromolecules*, 2007, **40**, 2897–2903.

70 R. S. Hoy, K. Foteinopoulou and M. Kröger, *Phys. Rev. E: Stat., Nonlinear, Soft Matter Phys.*, 2009, **80**, 031803.

71 N. C. Karayiannis and M. Kröger, *Int. J. Mol. Sci.*, 2009, **10**, 5054–5089.

72 C. Luo and J.-U. Sommer, *ACS Macro Lett.*, 2016, **5**, 30–34.

73 A. R. Khokhlov and S. K. Nechaev, *Phys. Lett. A*, 1985, **112**, 156–160.

74 V. Voevodin, A. Antonov, D. Nikitenko, P. Shvets, S. Sobolev, K. Stefanov, V. Voevodin, S. Zhumatiy, A. Brechalov and A. Naumov, *Contemporary High Performance Computing: From Petascale toward Exascale*, CRC Press, 2019, vol. 3, pp. 305–330.